Weber, T., Thomas, M. (2017): Influence of ocean tides on the general ocean circulation in the early Eocene. - *Paleoceanography*, *32*, 6, pp. 553—570.

DOI: http://doi.org/10.1002/2016PA002997

AGU PUBLICATIONS

Paleoceanography

RESEARCH ARTICLE
10.1002/2016PA002997

Influence of ocean tides on the general ocean circulation in the early Eocene

T. Weber[1] **and M. Thomas**[1,2]

[1]Helmholtz Centre Potsdam, GFZ German Research Centre for Geosciences, Section 1.3 Earth System Modelling, Potsdam, Germany, [2]Institute of Meteorology, Freie Universität Berlin, Berlin, Germany

Key Points:
- Horizontal velocities are increased significantly by tidal forcing in the early Eocene deep ocean
- The global meridional overturning circulation is strengthened by tidal dynamics
- Tidal forcing does not increase meridional heat transport sufficiently to reduce the meridional temperature gradient

Correspondence to:
T. Weber,
tobias.weber@gfz-potsdam.de

Citation:
Weber, T., and M. Thomas (2017), Influence of ocean tides on the general ocean circulation in the early Eocene, *Paleoceanography*, *32*, 553–570, doi:10.1002/2016PA002997.

Received 4 JUL 2016
Accepted 13 MAY 2017
Accepted article online 16 MAY 2017
Published online 15 JUN 2017

Abstract The early Eocene (~56–50 million years ago) was characterized by higher surface temperatures and a reduced meridional temperature gradient, compared to present-day conditions. The origin of the decreased meridional temperature gradient is still subject to discussion and might be linked to tides. Tidal mixing could have enhanced the meridional heat transport and thereby decreased the meridional temperature gradient. We test this hypothesis by simultaneously modeling tidal dynamics and the general ocean circulation for the early Eocene in a new coupled atmosphere-ocean model setup. We find an interaction between tidal currents and the ocean general circulation that increases horizontal velocities in 25% of the deep ocean to more than 400% of its original value. The global meridional overturning circulation is strengthened thereby locally by 60–100%. However, the oceanic meridional heat transport is only increased by a maximum of 0.1 PW (8%) and a mean of less than 0.018 PW (5.1%), thus not decreasing the meridional temperature gradient considerably.

1. Introduction

Analyzes of Mg/Ca ratios, $\delta^{18}O$ measurements, and TEX_{86} suggest early Eocene (EE, ~56–50 million years ago, Ma) sea surface temperatures between 27°C and 36°C in the tropics [*Lunt et al.*, 2012] and 10°C to 15°C in the polar oceans [*Zachos et al.*, 1994; *Ivany et al.*, 2008]. Although proxy-based reconstructions of polar surface temperatures are poorly constrained and show a considerable spread of 10°C [e.g., *Lunt et al.*, 2012], all reconstructions inferred a smaller equator-to-pole temperature gradient in the EE than today [e.g., *Zachos et al.*, 1994; *Greenwood and Wing*, 1995; *Barron*, 1987; *Tripati and Elderfield*, 2005]. This has not been adequately reproduced by paleoclimate simulations, so far [cf. *Lunt et al.*, 2012]. In order to solve the discrepancies between models and proxy data, a number of atmospheric and oceanic mechanisms that could increase polar temperatures have been suggested [*Bice and Marotzke*, 2002; *Tripati and Elderfield*, 2005; *Abbot and Tziperman*, 2008; *Kump and Pollard*, 2008; *Shellito et al.*, 2009; *Kiehl and Shields*, 2013], such as polar stratospheric clouds [*Sloan and Pollard*, 1998], vegetation-climate feedbacks [*Loptson et al.*, 2014], or the opening of the Arctic Ocean to its surrounding oceans [*Shellito et al.*, 2009]. However, none of these hypotheses has been able to effectively reduce the meridional temperature gradient to the values suggested by proxy data.

A prominent hypothesis about meridional heat redistribution states that a more efficient oceanic poleward heat transport could have warmed polar regions [*Barron*, 1987]. This hypothesis was rejected by *Sloan et al.* [1995] who found that an increase of poleward heat transport by 30% would be necessary to maintain high-latitude temperatures in the early Eocene, an increment that cannot be accomplished by the ocean circulation alone. However, *Green and Huber* [2013] theoretically derived that an intensification of the global meridional overturning circulation (GMOC) could have been achieved by tidal forcing of the ocean. A tidally strengthened GMOC would lead to an increased oceanic meridional heat transport that reduces the meridional temperature gradient. We test this hypothesis by including ephemeris tides into a new setup of the coupled atmosphere-ocean model ECHAM5/MPIOM (European Center Hamburg model version 5, Max Planck Institute ocean model) for the early Eocene.

Including tidal forcing into coupled atmosphere-ocean general circulation models helped *Lee et al.* [2006] and *Müller et al.* [2010] to improve the representation of present-day ocean currents and atmospheric near-surface temperatures. Nonetheless, the effects of tidal forcing are not included in most studies of the present-day climate [*IPCC*, 2013] and are neglected in both paleoclimate simulations and climate projections. Ocean tides instantaneously influence sea surface elevation and ocean velocities. Thereby, nonlinear processes

are induced that produce tidal residual mean currents that persist on climatological timescales. This shifts the direction of the flow paths of the mean ocean circulation and affects the velocities of ocean currents [*Munk et al.*, 1970; *Yanagi*, 1976; *Robinson*, 1981; *Zimmerman*, 1981; *Geyer and Signell*, 1990; *Aelbrecht et al.*, 1993]. Here we present a first study of the influence of ocean tides on ocean general circulation in the early Eocene and possible effects on climate. We will show that in the early Eocene tidal forcing mainly increases horizontal velocities in the deep ocean. Thereby, the GMOC is strengthened in the deep ocean, which influences meridional heat transport.

This manuscript is organized as follows. The coupled atmosphere-ocean model ECHAM5/MPIOM is described in section 2.1. The conditions of atmosphere and ocean during the early Eocene are presented and compared to a preindustrial climate simulation in section 3. The influence of tidal dynamics on ocean currents, oceanic temperature distribution, the GMOC, and atmospheric 2 m temperatures during the early Eocene are presented in section 4. We end with concluding remarks in section 5.

2. Models and Boundary Conditions

2.1. Models

The atmosphere and ocean circulation of a preindustrial period (PI) and the early Eocene are modeled with the coupled atmosphere-ocean global circulation model ECHAM5/MPIOM [*Roeckner et al.*, 2003, 2004; *Marsland et al.*, 2003; *IPCC*, 2013]. The setup used in this study follows *Uenzelmann-Neben et al.* [2016] and *Weber* [2016]. The atmosphere model ECHAM5 is applied with the horizontal resolution T31 ($\sim 3.75^\circ \times 3.75^\circ$) and 19 vertical hybrid sigma/pressure levels. ECHAM5 is coupled to the vegetation model JSBACH [cf. *Raddatz et al.*, 2007] for which we prescribe a heterogeneous vegetation distribution based on *Sewall et al.* [2000], *Huber and Sloan* [2001], and *Jungclaus* [2007]. A module for shortwave radiation is included in ECHAM5 according to *Fouquart and Bonnel* [1980]. The original implementation of the longwave radiation transfer scheme in ECHAM5 does not prevent occasional negative optical thicknesses, which would result in an increase of the radiative flux due to scattering or absorption, rather than a reduction of the flux along the original flux direction. Such nonphysical behavior has been prevented following *Heinemann* [2009] by setting the loss of energy in these cases to zero.

The Max-Plank-Institute Ocean Model (MPIOM) [*Marsland et al.*, 2003] solves the primitive equations for a hydrostatic Boussinesq fluid on an Arakawa-C-grid [*Arakawa and Lamb*, 1977; *Purser and Leslie*, 1988] with a horizontal resolution of $\sim 3.0^\circ \times 1.8^\circ$ and 20 unevenly distributed vertical levels (GR30L20). The vertical eddy viscosity and diffusion are parametrized by the Richardson number dependent scheme of *Pacanowski and Philander* [1981]. MPIOM includes a sea ice model that follows *Hibler* [1979] in the calculation of sea ice dynamics [*Marsland et al.*, 2003]. Furthermore, sea ice thermodynamics are taken into account, thus considering the alteration of the heat flux between ocean and atmosphere in the presence of sea ice and snow.

Earlier studies [*Thomas et al.*, 2001] show that the fast ocean dynamics induced by tidal forcing are affected by loading and self-attraction (LSA) of the water masses and that the inclusion of these processes into the ocean model increases the accuracy of modeled tidal amplitudes and phases. For this reason, LSA is included into MPIOM after an initial runup of 1500 years by applying the parametrization by *Accad and Pekeris* [1978] for the potential of LSA in the form

$$\Phi_{\mathrm{LSA}} = g\zeta \int_{-h}^{\eta} \frac{\rho(z)}{\rho_0} \mathrm{d}z, \tag{1}$$

where g is the mean gravitational acceleration, $\zeta = 0.1$ a proportionality factor [cf. *Parke*, 1982], η the instantaneous local sea surface elevation, h the ocean depth, ρ the instantaneous local density, ρ_0 a reference density, and z the vertical coordinate. Furthermore, the tidal module using an ephemeris approach to calculate the complete lunisolar tidal potential is included [*Thomas et al.*, 2001]. This model combination is run for further 100 years, of which the average over the last 50 years is analyzed in the following sections. In total, four simulations have been performed: the preindustrial and early Eocene simulations with consideration of LSA (named PICTRL and EECTRL) and with LSA and tidal forcing (named PITIDE and EETIDE).

Sensitivity studies by *Li et al.* [2012] for a similar model configuration as applied in our manuscript show that the deep ocean takes approximately 1000 years to reach a state of quasi-equilibrium and 5000 years for full equilibrium. Since such 5000 years long integrations are not feasible for most paleoclimatological studies,

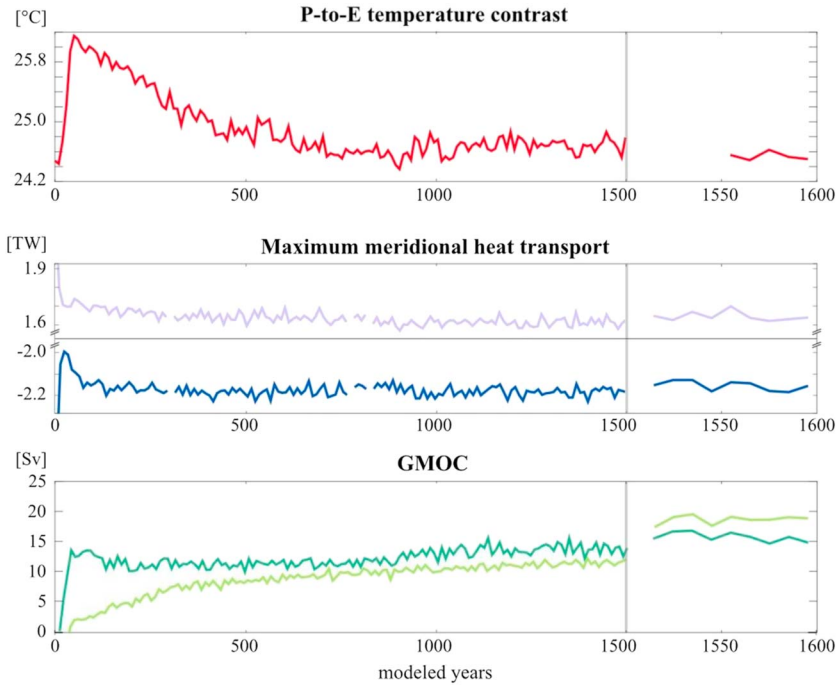

Figure 1. (red) Temporal evolution of pole-to-equator surface temperature contrast, maximum of the meridional heat transports in the (purple) Northern and (blue) Southern Hemispheres, and the global meridional overturning circulation at its maxima at (dark green) 35.5°N and 770 m depth and (light green) 18.5°S at 3700 m depth. The vertical gray line symbolizes the onset of tidal forcing. Gaps in the curves are missing data points.

an integration to the quasi-equilibrium is undertaken [e.g., *Poulsen et al.*, 2001; *Heinemann et al.*, 2009; *Winguth et al.*, 2010; *Lunt et al.*, 2012; *Stepanek and Lohmann*, 2012]. Figure 1 shows the temporal evolutions of the quantities analyzed in this study for the early Eocene: pole-to-equator surface temperature contrast, maximum of the oceanic meridional heat transports in both hemispheres, and the global meridional overturning circulation (GMOC) at its maxima in the Northern and Southern Hemispheres at 35.5°N at 770 m depth and at 18.5°S at 3700 m depth, respectively (cf. Figure 6). All variables show an adaptation phase during the first 1000 years. After simulation year 1000, the quantities stabilize and over the years 1300–1500 no statistically significant trend is evident. We conclude therefore that the model is in quasi-equilibrium after 1500 years. At this point tidal forcing and the parametrization of LSA are included. Once the ocean is forced by the tidal potential, a rapid change is visible in all control variables. After 50 years of tidal forcing (simulation year 1550), all quantities stabilize and no statistically significant trend remains.

2.2. Boundary Conditions

The atmospheric and vegetational boundary and initial conditions for PICTRL are based on experiment mil0001 [*Jungclaus*, 2007] of the Millennium Experiments performed by the Max-Planck-Institute for Meteorology. The CO_2 concentration is set to 278 ppm. Latitude-dependent ozone concentrations are prescribed according to *Fortuin and Kelder* [1998]. The ocean is initialized from the Polar Science Center Hydrographic Climatology [*Steele et al.*, 2001] projected onto the GR30L20 grid.

The model configuration applied for the early Eocene is similar to the one used by *Heinemann et al.* [2009]. However, different boundary conditions, such as topography, bathymetry, CO_2 concentration, orbital parameters, and vegetation distribution are applied in this study. We define boundary conditions for topography and vegetation based on global reconstructions from *Sewall et al.* [2000] and *Huber and Sloan* [2001]. We use a vegetation reconstruction with eight different plant functional types instead of a globally homogeneous vegetation for the EE. This way, local differences in vegetation and therefore albedo between EECTRL and PICTRL are considered. The concentration of CO_2 in the atmosphere is set to 450 ppm [cf. *Zeebe et al.*, 2009; *Pearson and Palmer*, 2000; *Royer et al.*, 2001; *Royer*, 2006]. Solar and orbital parameters were adapted to EE values following *Caldeira and Kasting* [1992], [*Laskar et al.*, 2004; 2011], and *Heinemann et al.* [2009].

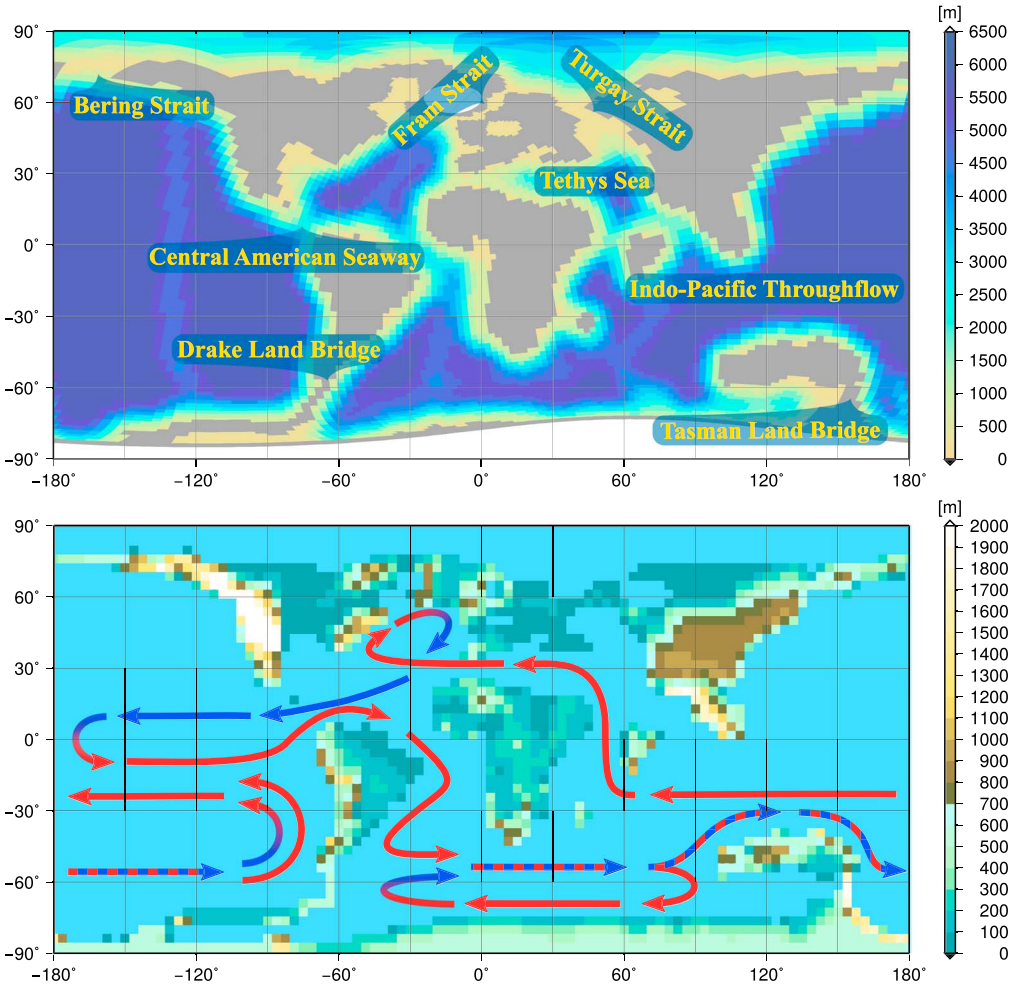

Figure 2. (top) Bathymetry and (bottom) topography for the EECTRL run used in the respective ocean and atmosphere model components. Arrows represent the global ocean conveyor belt as reconstructed from the EECTRL simulation. Red arrows indicate surface currents, blue arrows intermediate currents.

In analogy to PICTRL, the ocean grid poles are positioned over proto-Greenland and Antarctica. Apart from avoiding the singularities at the poles, this has the positive side effect that high resolution is obtained in areas where deep water formation is expected, such as in the Southern Ocean and Greenland Sea. The bathymetry reconstruction by *Sewall et al.* [2000] was projected onto this grid (Figure 2, top) [after *Uenzelmann-Neben et al.*, 2016], and the oceanic gateways and land bridges were adapted according to recent findings. The exact timing of the opening of the Drake Passage during the EE is controversially discussed [e.g., *Lawver and Gahagan*, 2003; *Livermore et al.*, 2005; *Ghiglione et al.*, 2008]. While an exchange of surface water between the South Atlantic and the Pacific Ocean might have been possible in the EE, a flow of intermediate and deep water was not possible. For this reason the Drake Passage is closed in our setup, therefore preventing the onset of a proto-Antarctic Circumpolar Current. *Iakovleva and Heilmann-Clausen* [2007] found *Wilsonidium pechoricum* on both sides of the Turgay Strait, indicating a seaway connecting intermittently the Tethys Sea and Arctic Ocean in the EE. The same conclusion is drawn by *Gleason et al.* [2009] for the Turgay, Bering, and Fram Straits by analyzing seawater Nd isotope values in the Arctic Ocean and the surrounding Oceans. For this reason, the Arctic Ocean is not completely isolated from the other ocean basins, as it is the case in the reconstructions by *Sewall et al.* [2000], but a throughflow of 200 m depth is created from the Arctic Ocean into the Pacific Ocean, the Tethys Sea, and the North Atlantic. This way, the transport of warm water into the Arctic Ocean is possible. The Tasmanian Gateway was closed during the EE, connecting Antarctica and Australia via a land bridge [*Scher and Martin*, 2006; *DeConto*, 2009]. Changing any of these discussed throughflows or land bridges can alter oceanic transports, temperature distribution, and currents. *Heinemann* [2009] used ECHAM5/MPIOM

with open Tasman and Drake Passages. Transports of 5 Sv (1 Sverdrup = 10^6 m^3 s^{-1}) were calculated at both passages. In comparison to 200 Sv and 140 Sv in their present-day simulation, these transports are negligible.

3. The Climate System

3.1. In the Preindustrial System

The average of the years 1550 to 1599 of PICTRL leads to a global annual mean surface temperature of 14.6°C, a sea surface temperature of 17.2°C, a precipitation of 2.9 mm d^{-1} and is therefore in good agreement with other simulation studies [*Lucarini and Russell*, 2002; *Zhang et al.*, 2012; *Compo et al.*, 2015]. The ocean dynamics are characterized by a vertically integrated transport by the Atlantic Meridional Overturning Circulation of 16.7 ± 0.7 Sv at 26°N which is somewhat less than the multiannual mean transport of 17.2 ± 0.9 Sv measured by *McCarthy et al.* [2015]. The transport by the Antarctic Circumpolar Current through the Drake Passage is simulated with 129±5.4 Sv which is in good agreement with *Cunningham et al.* [2003] who measure a transport of 134 ± 11.2 Sv. This implies that the coupled atmosphere-ocean model ECHAM5/MPIOM gives in the here presented setup a reasonable representation of present-day atmosphere and ocean conditions in comparison to other models and in situ measurements.

3.2. In the Early Eocene

In this section the results of EECTRL will be presented, analyzed, and compared to the results of other studies, some of which have been included by *Lunt et al.* [2012] into the Eocene Model Intercomparison Project (EoMIP) and involve four different atmosphere-ocean models (HadCAM, ECHAM5/MPIOM, Community Climate System Model (CCSM3), and Goddard Institute for Space Studies (ModelE-R)) with different boundary conditions and forcings.

3.2.1. Atmospheric Temperature Distribution

EECTRL shows a global annual mean surface temperature of 27.0°C and is thus 12.4°C warmer than the PI control run. Highest temperatures are found in the tropics of South America (45°C) and Africa (47°C, cf. Figure 3), while lowest temperatures occur in Antarctica with an averaged minimum of −6.5°C in austral winter. During local winter, snow depths of up to 32 cm are observed at the North American coasts and up to 10 cm in Antarctica, while both hemispheres are completely snow free during local summer. Largest differences in annual mean surface temperature between EECTRL and PICTRL are found in Antarctica, ranging from 35 to 69°C, Greenland (30 to 35°C) and the proto-Himalayan chain (35 to 43°C). Differences in altitude are responsible for a warming of up to 27°C in these areas, assuming a lapse rate of 6.5°C km^{-1}.

Similar temperatures have been simulated by *Winguth et al.* [2010], *Huber and Caballero* [2011], and *Kiehl and Shields* [2013] who performed sensitivity studies of the EE climate with respect to CO_2 concentrations and cloud properties using the CCSM. In order to obtain modeled surface temperatures that match proxy data and are similar to our model results, concentrations of CO_2 = 4480 ppm and CO_2 = 2250 ppm were necessary, i.e., one magnitude higher than the concentrations used in this study or in *Winguth et al.* [2012] with CCSM_H.

Heinemann et al. [2009], who used a concentration of CO_2 = 560 ppm, found a large increase of water vapor in the atmosphere due to high temperatures in the EE that primarily originate from increased CO_2 concentrations, compared to the PI simulations. This leads to a positive feedback, that is larger in ECHAM5 than in many other atmosphere models, such as CCSM used in *Winguth et al.* [2010], *Huber and Caballero* [2011], and *Kiehl and Shields* [2013]. In addition, planetary surface changes decreased albedo in their study and led to an increased surface temperature [cf. *Lunt et al.*, 2012]. This might explain why some models, such as ECHAM5 or CCSM_H, simulate surface temperatures that match proxy reconstructions at relatively low-CO_2 concentrations [cf. *Weber*, 2016].

3.2.2. Ocean

3.2.2.1. Temperature Distribution

While continental regions are on average by 15.4°C warmer in EECTRL than in PICTRL, the ocean's surface is only 9.7°C warmer. Strongest warming occurs in the polar oceans where annual mean sea surface temperatures (SSTs) above 8.0°C are obtained. In accordance with proxy data [e.g., *Pagani et al.*, 2006; *Sluijs et al.*, 2006], warm and brackish water can be found in the EE Arctic Ocean. In the western Pacific Ocean we find only a slight increase of SSTs, since an upwelling of cold water masses (cf. Figure 3) maintains low sea surface temperatures. Horizontal displacement of proto-Greenland relative to its current position is responsible for small surface temperature differences between EECTRL and PICTRL at the present-day location of Fram Strait. While in PICTRL surface temperatures are calculated at the sea level, in EECTRL the same location is characterized by an elevation of more than 600 m above sea level reducing the surface temperatures by at least 3.9°C.

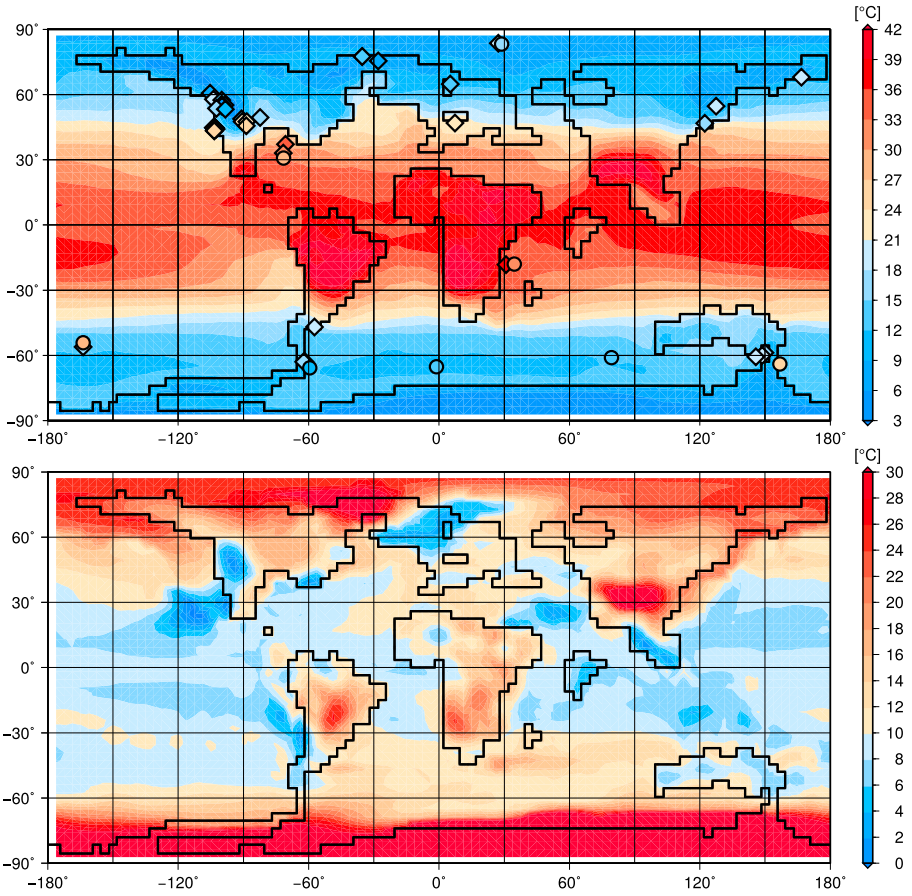

Figure 3. (top) Multidecadal mean surface temperature for EECTRL and (bottom) the difference EECTRL-PICTRL. Terrestrial (diamonds) and oceanic (circles) proxy data from *Huber and Caballero* [2011] and *Lunt et al.* [2012] are included.

In the EE, temperatures above freezing point lead to a sea ice free Arctic Ocean. Only in the Fram Strait a thin layer of sea ice forms in some winters. In agreement with earlier studies by *Heinemann et al.* [2009], *Stickley et al.* [2009], and *Pak and Miller* [1992], also, the Southern Ocean is completely ice free.

3.2.2.2. Formation of Deep and Intermediate Water

Warmer surface waters in the EE exert influence on deep water formation in polar regions. PICTRL shows convection depths of 1000–1500 m in the Weddell and Greenland Seas (not shown), whereas in EECTRL the convective depth is less than 300 m in the proto-Greenland Sea, the proto-Weddell Sea, the proto-Argentine basin, the proto-Ross Sea, and the Indo-Pacific Throughflow (Figure 4). Vertical profiles of vertical velocities (not shown) indicate downwelling to a depth of 3000 m in the proto-Weddell, proto-Ross, and proto-Greenland Seas. Comparing $\delta^{13}C$ values from four ocean basins, *Nunes and Norris* [2006] have concluded that the primary source of deep water in the EE was located in the Southern Oceans. This finding is specified by *Thomas et al.* [2014] to the Ross Sea, where also our model shows intermediate-water formation. This hypothesis is expanded by the results of numerical modeling by *Bice and Marotzke* [2001] who found that deep water formation occurred in the North Atlantic and the Southern Ocean. Another model by *Huber and Sloan* [2001] suggests deep water formation mainly in the Tethys Sea and the North Atlantic. In the Tethys Sea intermediate-water formation was also found by *Lunt et al.* [2010] who explained it by an increase in surface salinity due to high evaporation. In contrast, EECTRL shows stable stratification in the Tethys Sea and no sign of intermediate or deep water formation. Mixed layer depth of up to 250 m in the Argentine Basin and the Indo-Pacific Throughflow result from saline waters (cf. Figure 5) welling down to depths of 300–500 m.

3.2.2.3. Ocean Currents and the Global Ocean Conveyor Belt

In contrast to PICTRL, in EECTRL downwelling waters reach only maximum depths of 1500 m, thus leading to a shallower overturning circulation (Figure 6). Below 1500 m, currents are generally slower than 1.5 cm s^{-1},

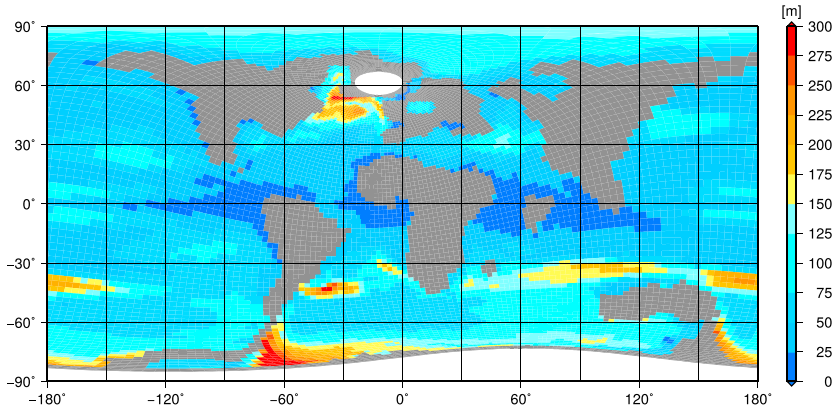

Figure 4. Depth of the mixed layer as modeled in EECTRL. Four areas of intermediate convection are visible: the proto-Greenland Sea, proto-Argentine Basin, proto-Ross Sea, and proto-Weddell Sea.

and the GMOC reaches a maximum of 13.4 Sv at a depth of approximately 800 m. In comparison hereto, the GMOC in PICTRL shows a maximum of 24.5 Sv at a depth of 1400 m and is present throughout the whole water column. A globally shallower circulation in the EE can be distinguished by examining the horizontal velocities at various throughflows, i.e., velocities around proto-India, in the Indo-Pacific Throughflow between Australia and Asia, and the Central American Seaway (Figure 2). In all cases no flow with velocities above 1.5 cm s^{-1} is developed below 1000 m, while strong currents of up to 15 cm s^{-1} are discernible in the upper 1000 m. This is in good agreement with the analysis of seismic profiles in the Argentine basin, for which small bottom velocities have been inferred [*Gruetzner et al.*, 2012; *Uenzelmann-Neben et al.*, 2016]. It also confirms the findings of previous studies [e.g., *Lunt et al.*, 2012, and references therein] that a vigorous ocean circulation with velocities larger than 1.5 cm s^{-1} was for the EE ocean below 1000 m.

The global ocean conveyor belt is driven by deep water formation in the proto-Greenland, proto-Weddell, and proto-Ross Seas (Figure 2). North Atlantic Deep Water is produced in the proto-Greenland Sea. As opposed to PICTRL, the EE simulation does not suggest a purely southward flow of North Atlantic Deep Water into the south Atlantic but a transport of 17.7 Sv through the Central American Gateway. The waters well up in the tropical Pacific and flow as surface currents through the South Atlantic into the southern proto-Indian Ocean. Here they split into a southern and a northern current, heading for the Pacific Ocean and the Weddell Sea, respectively. In the Weddell Sea, Antarctic Intermediate Water is formed. It flows through the southern part of the Indo-Pacific Throughflow into the South Pacific. Off the coast of South America, the Antarctic Intermediate Water wells up and, together with the surface current originating from the South Atlantic, flows back through the Indo-Pacific Throughflow at a rate of 91.8 Sv. The surface currents are partly transported through the Indian-African Throughflow into the Tethys Sea. From here, half of the surface water flows back into the Indian Ocean through the Indian-Asian Throughflow and induces a clockwise circulation around proto-India. The remaining half of the surface waters is transported to the proto-Greenland Sea at a rate of 18.3 Sv.

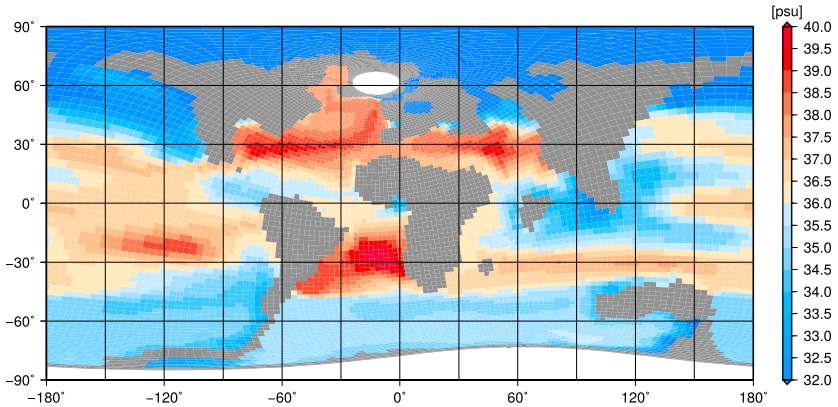

Figure 5. Multidecadal mean salinity for EECTRL at 10 m depth.

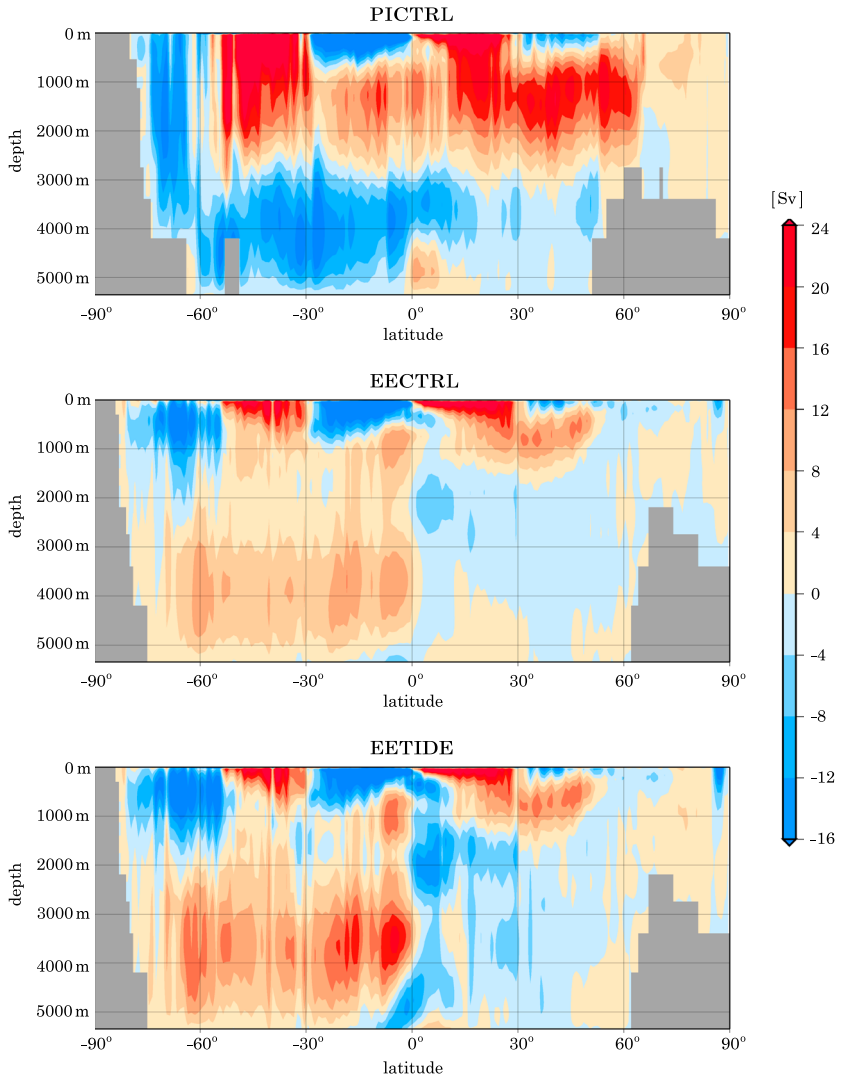

Figure 6. Global meridional overturning circulation (GMOC) for (top) PICTRL, (middle) EECTRL, and (bottom) EETIDE. Clockwise circulation is depicted red and positive; counterclockwise circulation blue and negative.

3.3. Comparison With Proxy Data

In order to validate the results of EECTRL we used globally distributed temperature proxy data from marine and onshore boreholes (Figure 3). These use different techniques such as Mg/Ca ratio analyzes, $\delta^{18}O$ measurements, and TEX_{86}, to reconstruct sea surface temperatures and land surface temperatures for the EE. The spatial distribution shows major discrepancies in reconstructed values between close proxies, i.e., in New Zealand where differences of 11°C exist between two close-by proxies. A perfect match between model and proxies can therefore not be expected.

The comparison shows that the simulation generally overestimates tropical surface temperatures by 2.1°C. This is especially the case for Caribbean and African sea surface temperatures (cf. Figure 3) although adjacent land surface temperatures are matched. Surface temperatures from the subtropical and temperate climate zones are underestimated by 4.5°C on average. However, the simulated land surface temperatures are within the error range of land proxies (Figure 7). Data coverage is dense in the Rocky Mountains, where uncertainty in paleoelevation leads to disparities between adjacent proxy records.

Discrepancies between simulated and reconstructed temperatures are especially large in the polar oceans: differences amount to more than ~10.0°C in New Zealand, Tasmania, and the Arctic Ocean (cf. Figure 3). This might be to a bias of the proxy data toward summer temperatures [*Eberle et al.*, 2010] or systematic errors in

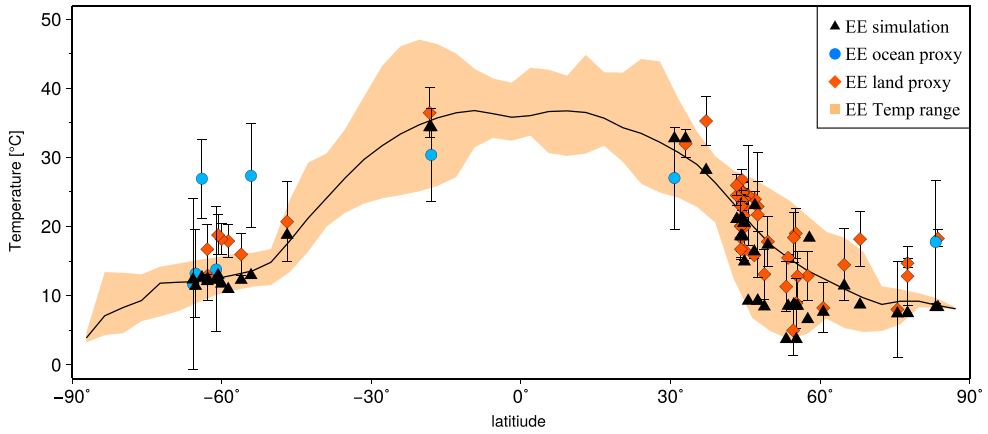

Figure 7. Zonally averaged modeled multidecadal mean surface temperature (solid black; SST over the ocean, air surface temperature over the continents). The orange shade marks the area between the zonal maximum and minimum of the multidecadal mean surface temperature of EECTRL, respectively. Included are terrestrial (diamonds) and oceanic (circles) proxies of the EE and the simulated values at the location of the proxy (triangle). Terrestrial proxy data are compiled by *Huber and Caballero* [2011] and provided by *Lunt et al.* [2012]; oceanic proxy data are compiled and provided by *Lunt et al.* [2012].

the correlation between TEX_{86} and SSTs [*Ho and Laepple*, 2015]. *Ho and Laepple* [2016] point out that TEX_{86} should not be calibrated against SSTs but rather subsurface waters (0–200 m depth). This questions TEX_{86} as a proxy for SSTs.

Proxy data suggest an equator-to-pole temperature gradient of under 20°C. The meridional temperature contrast $\Delta T = T(|\phi| < 30°) - T(|\phi| > 60°)$, with latitude ϕ, [cf. *Lunt et al.*, 2012] is 24.6°C in EECTRL and, thus, about 14.6°C lower than in PICTRL with $\Delta T = 39.2$°C. Nevertheless, the meridional temperature gradient is still significantly higher than suggested by proxy data. This is a well-known problem in paleoclimate simulations and has also been found in other modeling studies [e.g., *Heinemann et al.*, 2009; *Lunt et al.*, 2012]. However, new evidence suggests that the discrepancy does originate not only from model deficiencies but also from misinterpretation of proxy data [*Ho and Laepple*, 2016]. The meridional temperature gradient inferred from the current model experiment is in similar or better agreement with proxy data than other studies that apply relatively low concentrations of CO_2 [cf. *Lunt et al.*, 2012].

4. Tidal Dynamics

4.1. Tides in the Preindustrial Period

The skill of the tidal model can be estimated by comparison of the tidal simulation of a preindustrial period PITIDE with in situ measurements. Figure 8 shows the amplitude and phase of the M_2 partial tide as simulated in PITIDE. Highest amplitudes of up to 2.0 m are modeled in the coastal areas of the northern Pacific, the Weddell Sea, the Hudson Strait, the eastern North Atlantic, the Mozambique Channel, and north of Australia. Comparison of the amplitudes of the modeled partial tides M_2 and K_1 with the tide-gauge data set ST103 [*Le Provost et al.*, 1994] gives a root-mean-square error of 18.3 cm and 7.2 cm, respectively. Applying the same ocean model with an increased horizontal resolution, *Müller et al.* [2010] obtained a root-mean-square error of 12.9 cm and 4.8 cm for the amplitudes of M_2 and K_1 partial tides, respectively, in comparison to ST103. The higher accuracy is due to the higher spatial resolution used by *Müller et al.* [2010], which is not applicable for long-term paleosimulations. MPIOM and the tidal module by *Thomas et al.* [2001] give therefore a reasonable representation of global tides, considering the coarse resolution required by paleomodeling [cf. *Weber*, 2016].

4.2. Tides in the Early Eocene

The differences in bathymetry during the early Eocene and present-day affect the geometry and resonance conditions of ocean basins [cf. *Weber*, 2016]. Thereby, amplitudes of partial tides are altered, and consequently, the amphidromic systems are shifted (Figure 8). The Indian Ocean is of smaller extend in the early Eocene due to the more southern locations of India and Australia. The Tethys Sea is open and connects the North Atlantic with the Indian Ocean. Several amphidromic points of the M_2 partial tide are positioned over proto-India where they lead to small tidal amplitudes of less than 50 cm in the central Indian Ocean and produce large

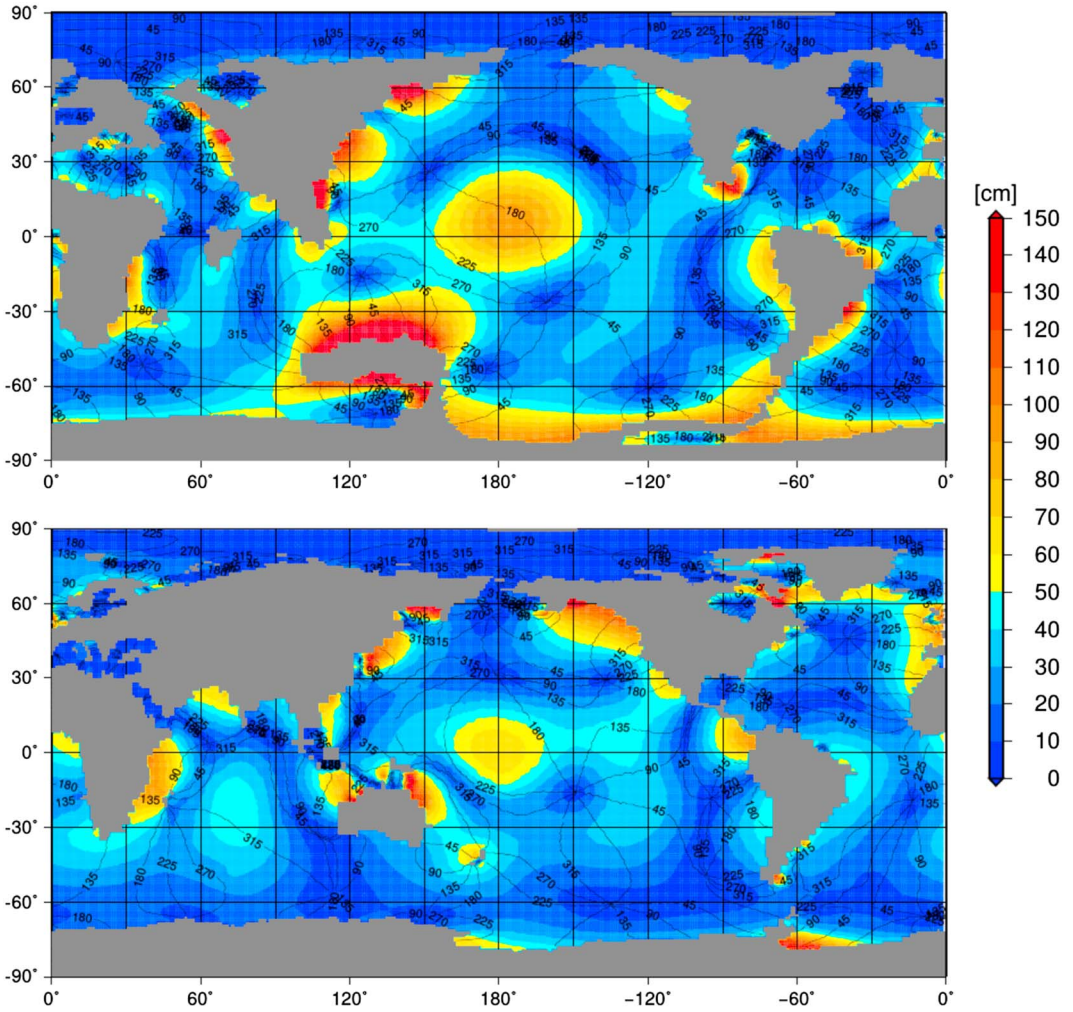

Figure 8. Amplitude (colored contours) and phase (numbered lines in degrees) of the M_2 partial tide calculated by least squares errors from the simultaneous runs of circulation and ephemeris tides for the early Eocene (EETIDE, top) and the pre-industrial period (PITIDE, bottom). The phase is relative to Greenwich Mean Time.

amplitudes of more than 1 m at the coasts. The proto-Australian coast is influenced by three tidal systems formed by a Kelvin wave traveling around Australia counterclockwise. Thereby, large amplitudes of the M_2 partial tide of up to 4 m and strong tidal residual mean currents are induced. The shallow Tethys Sea is dominated by five small-scale amphidromic systems with small amplitudes and moderate tidal residual mean currents. The positions of the amphidromic systems in the Pacific Ocean and the North Atlantic are similar in EETIDE and PITIDE, although amplitudes in the central Pacific are with almost 1 m twice as high in EETIDE than in PITIDE.

Green and Huber [2013] used the Oregon State University Tidal Inversion System to simulate tides in the early Eocene. They found a dependence of the modeled tidal amplitudes on the prescribed ocean stratification. The position of amphidromic points, however, is independent of the ocean stratification. The amplitudes of the M_2 partial tide in EETIDE are most similar to the simulations by *Green and Huber* [2013] with EE topography and preindustrial stratification. Largest amplitudes are obtained in both simulations in the central and North Pacific; the northern Central American Seaway and close to Australia where expanded and deeper Pacific and Indian Ocean basins and a wider Indo-Pacific Throughflow generate favorable resonance conditions (Figure 8). The narrower EE Atlantic, on the other hand, leads to a multiplicity of amphidromic systems with smaller amplitudes in EETIDE than in PITIDE. Small differences in bathymetries between EETIDE and *Green and Huber* [2013] lead to a shift from highest amplitudes surrounding Australia in EETIDE to high amplitudes around New Zealand in *Green and Huber* [2013]. Furthermore, the open Drake Passage and Tasman Gateway

in *Green and Huber* [2013] allow tidal waves to travel unobstructed in the Southern Oceans. In EETIDE, these two gateways are closed, inhibiting the propagation of tidal waves and forming a Kelvin wave at the continental borders.

We expect the main discrepancies between *Green and Huber* [2013] and EETIDE to derive from differences in bathymetry reconstructions and the assumed ocean stratification. Hence, they reflect the uncertainty of simulated paleotidal systems due to bathymetry reconstructions and ocean stratification. The quantitative results presented in this study should therefore be considered as a means to derive qualitative and comparative conclusions. Further uncertainty is brought into the ocean model by the variations of orbital parameters of Sun, Moon, and Earth on geological timescales [*Laskar et al.*, 2004, 2011]. However, they alter amplitudes of the M_2 partial tide in the global mean by only 4% during the early Eocene [*Weber*, 2016] and are hence neglected in EETIDE. Nevertheless, this effect becomes significant for longer time periods and should be considered in future studies.

4.2.1. Effect of Ocean Tides on the Mean General Circulation

Differences in horizontal velocities between EETIDE and EECTRL are produced by (1) tidal residual mean currents (TRMCs) and (2) increased vertical mixing. TRMCs are the consequence of nonlinear interaction between tidal currents and atmosphere, topography, and other currents. They are therefore largest at the surface and the bottom. Increased vertical mixing mainly strengthens the existing thermohaline currents.

Largest differences in horizontal velocities between EETIDE and EECTRL are located at the surface (cf. Figure 9, middle). This is due to the combined effects of TRMC and tidally altered atmosphere forcing, e.g., wind stress [cf. *Weber*, 2016]. Differences in currents between EETIDE and EECTRL of up to 9 cm s^{-1} occur. In the 50 year mean, absolute changes in horizontal velocities are most pronounced in the tropics and the polar oceans. However, wind-driven surface velocities are larger than the TRMC, and the fraction EETIDE/EECTRL is limited to changes of 20% in most of the upper ocean (cf. Figure 9, top right).

In the deep ocean, water currents are rarely stronger than 1 cm s^{-1} below 3000 m depth, whereas the inclusion of tidal forcing leads to mean velocities of more than 2 cm s^{-1} in EETIDE (cf. Figure 9, bottom left). This is majorly the case in areas where tidal amplitudes are large, e.g., in the Indo-Pacific Throughflow, the North Atlantic, and the Southern Ocean. Horizontal velocities at 2750 m depth are changed by increased vertical mixing and TRMC by more than 80% in 90% of the ocean and quadrupled in 25% of the ocean.

Influence of tides on ocean circulation can also be seen in the preindustrial simulations. Including tides into the ocean model MPIOM improved the representation of the North Atlantic Current in *Müller et al.* [2010]. Thereby, also, the advection of heat by the Gulf Stream is simulated more accurately which leads to an improved reproduction of SST distribution. Influence of tides on surface temperatures and sea ice concentration is obtained by several models especially for the Arctic and Southern Oceans [*Koentopp et al.*, 2005; *Lee et al.*, 2006; *Holloway and Proshutinsky*, 2007]. Tides are thus a nonnegligible component of the climate system because they affect ocean currents, temperature, and sea ice on the short term and long term. Comparing the simulations of the early Eocene and present-day shows that horizontal velocities in the deep ocean are stronger affected by tidal forcing in EETIDE than in PITIDE. Tidal forcing increases vertical mixing and invigorates thereby the thermohaline circulation. In PICTRL already a strong vertical mixing is simulated and tidal forcing has therefore little effect on mixing. Hence, the thermohaline circulation is only strengthened slightly in PITIDE. In EECTRL, on the other hand, less vertical mixing is simulated than in PICTRL and the relative increase of mixing in EETIDE due to tidal forcing is larger than in the preindustrial. Therefore, the intensification of the thermohaline circulation is stronger in EETIDE than in PITIDE, and absolute and—to an even larger extend—relative velocity differences between EETIDE and EECTRL are larger than the differences between PITIDE and PICTRL [cf. *Weber*, 2016].

4.2.2. The Influence of Tides on the Meridional Overturning Circulation

The patterns of the global meridional overturning circulation (GMOC) are similar in EETIDE and EECTRL (Figure 6). Their magnitude, however, is increased by 6–10 Sv (60–100%) below a depth of 2000 m in EETIDE compared to EECTRL due to increased meridional velocities. The intensification of the GMOC is especially large in the Southern Hemisphere deep ocean overturning cell (maximum of 10 Sv at a depth of 3500 m) and in the Northern Hemisphere intermediate ocean (6 Sv, 2000 m). In EECTRL, the meridional stream function shows a separation of the dynamical system of the upper 2000 m from the deep ocean. In EETIDE this separation is less pronounced, and the stronger overturning cells indicate an increased mixing between the deep ocean and the intermediate ocean, especially in the Southern Oceans and the North Atlantic. The temporal evolutions

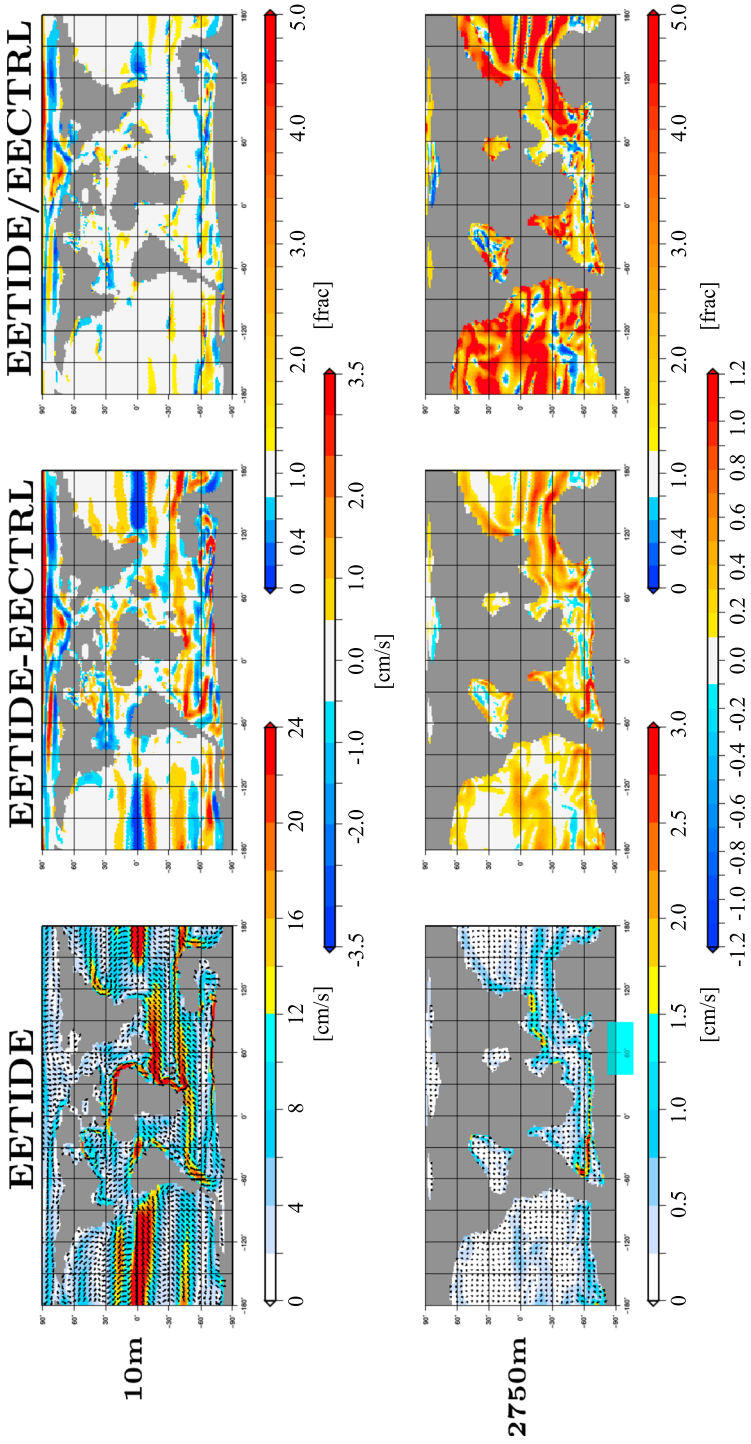

Figure 9. Horizontal velocities of (left column) EETIDE, (middle column) their absolute difference EETIDE-EECTRL, and (right column) their fraction EETIDE/EECTRL at 10 m (top) and 2750 m (bottom) depths of the 50 year mean of the early Eocene simulations.

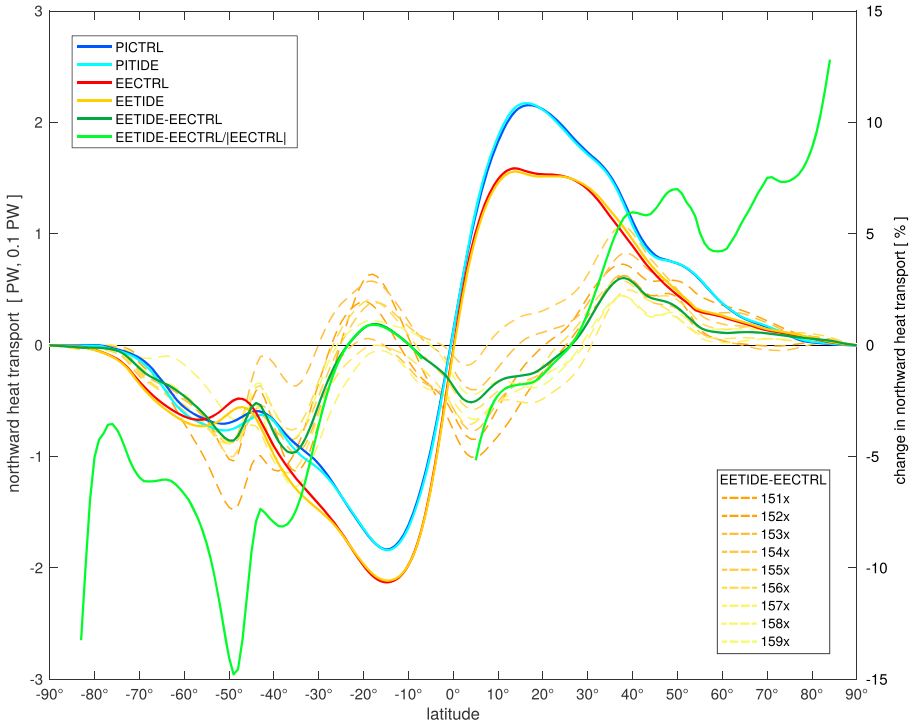

Figure 10. Northward oceanic heat transport in PW for the experiments (dark blue) PICTRL, (light blue) PITIDE, (red) EECTRL, (orange) EETIDE, (dark green) the difference EETIDE-EECTRL in 0.1 PW, and (light green, right *y* axis) the percentage change (EETIDE-EECTRL)/|EECTRL|. The difference EETIDE-EECTRL in MHT for decadal means from 151x to 159x is given in dashed orange and yellow lines in 0.1 PW (changing gradually from orange for 151x to yellow for 159x).

of two local maxima of the GMOC show that the onset of tidal forcing increases the GMOC over a period of 50 years, after which a new quasi-equilibrium is reached (Figure 1). Slight trends of −0.038 Sv and 0.0036 Sv per year are simulated for the GMOC at depths of 770 m and 3700 m, respectively. According to a Student's *t* test, these trends are statistically not significant.

Green and Huber [2013] argued that the tidally increased vertical mixing would increase the GMOC and thereby the meridional heat transport (MHT). They concluded that including tidal forcing into a coupled atmosphere-ocean global circulation model should therefore result in a decrease of the meridional surface temperature gradient. In our simulations the GMOC is increased by tidal forcing in agreement with *Green and Huber* [2013]. However, the meridional heat transport is increased in the Northern Hemisphere by a maximum of 0.06 PW (6%) and a mean of 0.006 PW which corresponds to 4.4%. In the Southern Hemisphere the transport is increased by a maximum of 0.1 PW (8%) with a mean of 0.03 PW (corresponding to 5.7%, Figure 10). The meridional temperature contrast ΔT is in EETIDE only 0.1°C lower than in EECTRL and has a value of 24.5°C. This might be caused by an intensification of the GMOC below 1000 m depth and no significant changes in the upper 1000 m. Thereby, water masses are mixed more intensely in the deep ocean, while they keep being separated from the surface. This is in contrast to findings by *Thomas et al.* [2014] who determined that especially augmenting mixing in the abyssal ocean increases the meridional heat transport and reduces the meridional surface temperature gradient. We reckon that the differences most likely originate in different structures of the GMOC. *Thomas et al.* [2014] simulate deep water formation at the northern and southern rim of the Pacific Ocean. In our simulations deep water is mainly formed in the Greenland Sea and the Weddell Sea, with very little contribution from the southern Pacific. The different formation of deep water in the two studies induces different overturning cells. *Thomas et al.* [2014] simulate in each hemisphere one overturning cell spanning from the surface to at least 4000 m depth. These overturning cells gain in strength with an increase in vertical mixing (e.g., by tidal forcing) and transport more warm surface waters to high latitudes. Thereby, the meridional heat transport is increased. In EECTRL and EETIDE in each hemisphere upper and lower overturning cells are simulated, separated between 1500 and 2000 m depth (cf. Figure 6). Tidal forcing does not only strengthen the poleward transport of warm surface waters but also

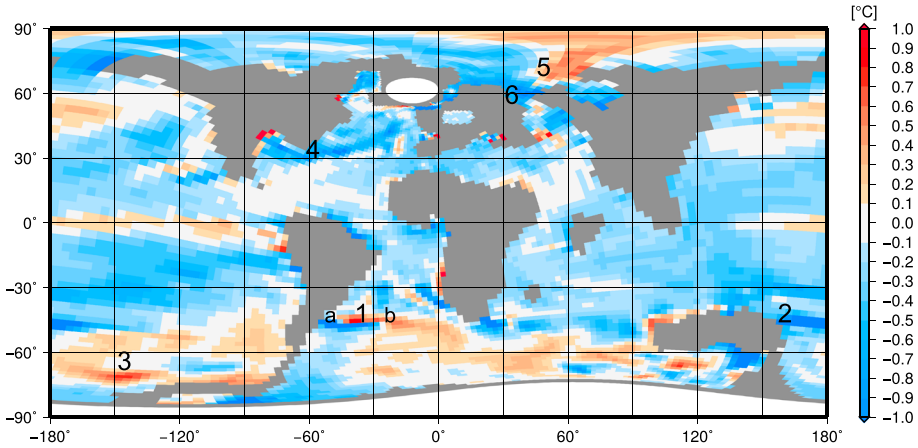

Figure 11. Difference EETIDE-EECTRL in ocean temperature at a depth of 10 m. Numbers indicate areas with exceptional temperature changes in the EETIDE experiment compared to EECTRL.

the equatorward transport of intermediate waters. Averaging vertically, the meridional heat transport is only slightly affected by tides (cf. Figure 10). The initial shock received by the model by abruptly turning on tidal forcing leads to largest differences in MHT at the beginning of the onset of the tidal forcing (indicated by the difference EETIDE-EECTRL in Figure 10 in orange). Over time, the difference between EETIDE and EECTRL gets smaller and converges toward the 50 year mean (indicated in dark green in Figure 10).

Rose and Ferreira [2013] find that an increased poleward oceanic heat transport is counteracted by a decreased atmospheric heat transport. According to their study, the primary effect of ocean heat transport on the meridional temperature gradient is by modulation of deep moist convection in the midlatitude storm tracks. Accordingly, for a reduction of the meridional temperature gradient the oceanic polar heat transport in the midlatitudes is of importance. This is only slightly increased by a maximum of 7% in the Northern Hemisphere and 15% in the Southern Hemisphere.

The tidally forced strengthening of vertical mixing could also increase the ventilation of the deep ocean and decrease the carbon storage capacity in the deep ocean [cf. *Marinov et al.*, 2008; *Marinov and Gnanadesikan*, 2011]. This storage capacity could vary over time as found by *Sexton et al.* [2011] when investigating the Eocene concentration of $CaCO_3$ in drill cores from the West and South Atlantic and the Pacific Ocean. They found periodic releases of CO_2 which they linked to periodic ventilation of the deep ocean. The increased strength of the GMOC in EETIDE indicates that tidal forcing might have an impact on the CO_2 storage capacity of the deep ocean.

4.2.3. Effect of Ocean Tides on Near-Surface Temperatures

Tidal alteration of advection and vertical mixing modify SSTs. In EETIDE, ocean temperatures in 10 m depth decline by 0.2°C on a global scale compared to EECTRL, with a moderate decrease in most oceans, especially the tropical regions (cf. Figure 11). Six areas of large temperature deviations have been identified (cf. Figure 11) in the moderate and arctic climate zones.

Tidal dynamics in the southern South Atlantic strengthen surface currents from the Southern Ocean into the Atlantic Ocean in EETIDE, thus transporting cold water into the Argentine basin and decreasing temperatures by up to 2.5°C ((1a) in Figure 11). In addition to increased velocity, this current is directed more toward the west and less to the north in EETIDE than in EECTRL (cf. Figure 9). Hereby, the influence of Southern Ocean water is decreased in the eastern South Atlantic, whereas the warmer waters from the equatorial regions of the South Atlantic gain in influence and slightly warm the eastern South Atlantic by 0.5°C (1b). In the area east of Australia (2), tidal residual mean currents strengthen the clockwise circulation and transport additional cold water from the coast of Antarctica to the midlatitudes and thereby decrease temperatures by almost 2°C. On the other side of the Pacific Southern Ocean, tidal forcing strengthens the general ocean circulation and increases transport of warm waters from the Pacific Ocean into the Southern Ocean (3).

In the North Atlantic, the Gulf Stream is weakened by a counterclockwise rotating amphidromic system. Hereby, less warm water from the tropics is transported into the North Atlantic (4), decreasing temperatures by more than 1°C. In the Arctic Ocean currents are modified in a similar way by an amphidromic system.

The counterclockwise circulation transports warm water from the proto-Kara Sea into the Arctic Ocean (5), and cold water from the Arctic Ocean into the Turgay Strait (6). This leads to a by 0.5°C warmer Arctic Ocean and a by 1°C colder Turgay Strait in EETIDE than in EECTRL.

5. Conclusions

Steady state dynamics of the atmosphere and ocean have been simulated with the coupled atmosphere-ocean model ECHAM5/MPIOM for a time slice of the early Eocene. In accordance with proxy data, the model simulations suggest a warm and humid climate in the EE with a global mean surface temperature of 27.0°C (Figure 7). Although the meridional temperature gradient is considerably decreased in our simulations of the early Eocene compared to the preindustrial period, the poles are not warmed to the extent suggested by proxy data. This indicates that some processes responsible for polar warming of meridional heat redistribution might still be missing in atmosphere-ocean models. However, also, the possibility of systematic errors in the correlation between TEX_{86} and sea surface temperatures cannot be discarded [*Ho and Laepple*, 2015].

Green and Huber [2013] suggested tidal forcing as a driver of increased meridional heat transport and thus as a reason for reduced meridional temperature gradients. In order to test their hypothesis, we included tidal forcing into ECHAM5/MPIOM and performed two simulations considering (EETIDE) and neglecting tides (EECTRL). Tidal residual mean currents impact the ocean general circulation in the EE especially in the deep ocean. While almost no currents faster than 1 cm s^{-1} are modeled below 1000 m in EECTRL, velocities of up to 3 cm s^{-1} are simulated in EETIDE at the ocean bottom. In 25% of the deep ocean a quadrupling of horizontal velocities is simulated in EETIDE compared to EECTRL. The increased meridional velocities strengthen the GMOC by up to 100% in the Southern Hemisphere deep ocean. However, the meridional heat transport is only slightly increased in the Northern Hemisphere by mean of 0.006 PW (4.4%) and in the Southern Hemisphere by 0.03 PW (5.7%). The meridional temperature gradient ΔT is thereby reduced by only 0.1°C. The hypothesis by *Green and Huber* [2013] and *Thomas et al.* [2014] that tidal forcing can decrease the meridional temperature gradient in the EE is therefore not supported by our simulations, and tides did not significantly contribute to a reduced meridional temperature gradient in the early Eocene. The differences between the study by *Thomas et al.* [2014] and our simulations might originate from different vertical structures of the meridional overturning circulation. While *Thomas et al.* [2014] simulate one overturning cell in each hemisphere, in our simulations one upper and one lower overturning cells are simulated in each hemisphere. We can therefore not eliminate the possibility that in a model that simulates one large vertical overturning cell in each basin or hemisphere, tidal mixing possibly could increase meridional heat transport.

Although tidal dynamics are sensitive to the bathymetry and thus the modeling of paleotides is constrained by the quality of bathymetry reconstructions, our study gives an impression of the effect tidal dynamics have on the ocean's general circulation in the EE. The effects of tides on horizontal ocean bottom velocities and the GMOC are considerable. Tidal dynamics should therefore be taken into consideration as a source of uncertainty for the interpretation of paleo-ocean simulations.

Acknowledgments
We thank Helmuth Haak for his help in setting up the ocean model for PI and EE runs and Jacob O. Sewall for the boundary conditions for the EE run. We are grateful to I. Rogozhina and J. Saynisch for fruitful discussions and revisions. We thank the reviewers and the Editor for their thoughtful comments. The model experiments were carried out on the supercomputing system of the German Climate Computation Centre (DKRZ) Hamburg. This study is funded by the Deutsche Forschungsgemeinschaft (DFG) under grant TH 864/11 as part of the priority program SPP 1375 SAMPLE (South Atlantic Margin Processes and Links with onshore Evolution). Data supporting the figures are available at http://doi.org/10.5880/GFZ.1.3.2017.001 [*Weber and Thomas*, 2017].

References

Abbot, D. S., and E. Tziperman (2008), Sea ice, high-latitude convection, and equable climates, *Geophys. Res. Lett.*, *35*, L03702, doi:10.1029/2007GL032286.

Accad, Y., and C. L. Pekeris (1978), Solution of the tidal equations for the M_2 and S_2 tides in the world oceans from a knowledge of the tidal potential alone, *Philos. Trans. R. Soc. A*, *290*(1368), 235–266, doi:10.1098/rsta.1978.0083.

Aelbrecht, D., G. Chabert D'Hieres, and X. Zhang (1993), Generation of a residual current by interaction between the coastal boundary layer and the Ekman layer in a tidal motion, *Oceanol. Acta*, *16*(5–6), 479–487.

Arakawa, A., and V. R. Lamb (1977), Computational design of the basic dynamical processes of the UCLA general circulation model, *Meth. Comput. Phys.*, *14*, 173–265.

Barron, E. J. (1987), Eocene equator-to-pole surface ocean temperatures: A significant climate problem?, *Paleoceanography*, *2*(6), 729–739.

Bice, K. L., and J. Marotzke (2001), Numerical evidence against reversed thermohaline circulation in the warm Paleocene/Eocene ocean, *J. Geophys. Res.*, *106*(C6), 11,529–11,542, doi:10.1029/2000JC000561.

Bice, K. L., and J. Marotzke (2002), Could changing ocean circulation have destabilized methane hydrate at the Paleocene/Eocene boundary?, *Paleoceanography*, *17*(2), 1018, doi:10.1029/2001PA000678.

Caldeira, K., and J. F. Kasting (1992), The life span of the biosphere revised, *Nature*, *360*(24), 721–723.

Compo, G., J. Whitaker, P. Sardeshmukh, N. Matsui, R. Allan, X. Yin, B. Gleason, R. Vose, G. Turledge, and P. Bessemoulin (2015), *NOAA/CIRES Twentieth Century Global Reanalysis Version 2c*, Comput. and Inf. Syst. Lab., Natl. Cent. for Atmos. Res., Univ. Corp. for Atmos. Res., Boulder, Colo.

Cunningham, S., S. G. Alderson, B. A. King, and M. A. Brandon (2003), Transport and variability of the Antarctic Circumpolar Current in Drake Passage, *J. Geophys. Res.*, *108*(C5), 8084, doi:10.1029/2001JC001147.

DeConto, R. M. (2009), Plate tectonics and climate change, in *Encyclopedia of Paleoclimatology and Ancient Environments, Encycl. of Earth Sci. Ser.*, edited by V. Gornitz, pp. 1049–1064, Springer, Netherlands.

Eberle, J. J., H. C. Fricke, J. D. Humphrey, L. Hackett, M. G. Newbrey, and J. H. Hutchison (2010), Seasonal variability in Arctic temperatures during early Eocene time, *Earth Planet. Sci. Lett.*, *296*(3–4), 481–486, doi:10.1016/j.epsl.2010.06.005.

Fortuin, J. P. F., and H. Kelder (1998), An ozone climatology based on ozonesonde and satellite measurements, *J. Geophys. Res.*, *103*(D24), 31,709–31,734.

Fouquart, Y., and B. Bonnel (1980), Computations of solar heating of the Earth's atmosphere: A new parameterization, *Beitr. Phys. Atmos.*, *53*, 35–62.

Geyer, W. R., and R. Signell (1990), Measurements of tidal flow around a headland with a shipboard acoustic Doppler current profiler, *J. Geophys. Res.*, *95*(C3), 3189–3197.

Ghiglione, M. C., D. Yagupsky, M. Ghidella, and V. A. Ramos (2008), Continental stretching preceding the opening of the Drake Passage: Evidence from Tierra del Fuego, *Geology*, *36*(8), 643–646, doi:10.1130/G24857A.1.

Gleason, J. D., D. J. Thomas, T. C. Moore Jr, J. D. Blum, R. M. Owen, B. A. Haley, and PA2215 (2009), Early to middle Eocene history of the Arctic Ocean from Nd-Sr isotopes in fossil fish debris, Lomonosov Ridge, *Paleoceanography*, *24*, PA2215, doi:10.1029/2008PA001685.

Green, J. A. M., and M. Huber (2013), Tidal dissipation in the early Eocene and implications for ocean mixing, *Geophys. Res. Lett.*, *40*, 2707–2713, doi:10.1002/grl.50510.

Greenwood, D. R., and S. L. Wing (1995), Eocene continental climates and latitudinal temperature gradients, *Geology*, *23*(11), 1044–1048.

Gruetzner, J., G. Uenzelmann-Neben, and D. Franke (2012), Variations in sediment transport at the central Argentine continental margin during the Cenozoic, *Geochem. Geophys. Geosyst.*, *13*, Q10003, doi:10.1029/2012GC004266.

Heinemann, M. (2009), Warm and sensitive Paleocene-Eocene climate, PhD thesis, Univ. of Hamburg, Hamburg, Germany.

Heinemann, M., J. H. Jungclaus, and J. Marotzke (2009), Warm Paleocene/Eocene climate as simulated in ECHAM5/MPI-OM, *Clim. Past*, *5*, 785–802.

Hibler, W. D. (1979), A dynamic thermodynamic sea ice model, *J. Phys. Oceanogr.*, *9*, 815–846.

Ho, S. L., and T. Laepple (2015), Glacial cooling as inferred from marine temperature proxies TEX_{86}^{H} and $U_{37}^{K'}$, *Earth Planet. Sci. Lett.*, *409*, 15–22, doi:10.1016/j.epsl.2014.10.033.

Ho, S. L., and T. Laepple (2016), Flat meridional temperature gradient in the early Eocene in the subsurface rather than surface ocean, *Nat. Geosci.*, *9*, 606–613, doi:10.1038/NGEO2763.

Holloway, G., and A. Proshutinsky (2007), Role of tides in Arctic Ocean/ice climate, *J. Geophys. Res.*, *112*, C04S06, doi:10.1029/2006JC003643.

Huber, M., and R. Caballero (2011), The early Eocene equable climate problem revisited, *Clim. Past*, *7*(2), 603–633, doi:10.5194/cp-7-603-2011.

Huber, M., and L. C. Sloan (2001), Heat transport, deep waters, and thermal gradients: Coupled simulation of an Eocene greenhouse climate, *Geophys. Res. Lett.*, *28*(18), 3481–3484, doi:10.1029/2001GL012943.

Iakovleva, A. I., and C. Heilmann-Clausen (2007), Wilsonidium Pechoricum new species—A new Dinoflagellate species with unusual asymmetry from the Paleocene/Eocene Transition, *J. Paleontol.*, *81*(5), 1020–1030, doi:10.1666/pleo05-120.1.

IPCC (2013), *Climate Change 2013: The Physical Science Basis. Contribution of Working Group I to the Fifth Assessment Report of the Intergovernmental Panel on Climate Change*, 1–1535 pp., Cambridge Univ. Press, Cambridge, U. K., and New York.

Ivany, L. C., K. C. Lohmann, F. Hasiuk, D. B. Blake, A. Glass, R. B. Aronson, and R. M. Moody (2008), Eocene climate record of a high southern latitude continental shelf: Seymour Island, Antarctica, *Geol. Soc. Am. Bull.*, *120*(5–6), 659–678, doi:10.1130/B26269.1.

Jungclaus, J. H. (2007), *MPI-M Earth System Modelling Framework: Millennium Control Experiment*, World Data Center for Climate, CERA-DB "mil0001", DKRZ. [Available at http://cera-www.dkrz.de/WDCC/ui/Compact.jsp?acronym= mil0001.]

Kiehl, J. T., and C. A. Shields (2013), Sensitivity of the Palaeocene-Eocene Thermal Maximum climate to cloud properties, *Philos. Trans. R. Soc. A*, *371*, 20130093, doi:10.1098/rsta.2013.0093.

Koentopp, M., O. Eisen, C. Kottmeier, L. Padman, and P. Lemke (2005), Influence of tides on sea ice in the Weddell Sea: Investigations with a high-resolution dynamic-thermodynamic sea ice model, *J. Geophys. Res.*, *110*, C02014, doi:10.1029/2004JC002405.

Kump, L. R., and D. Pollard (2008), Amplification of Cretaceous warmth by biological cloud feedbacks, *Science*, *320*(5873), 195, doi:10.1126/science.1153883.

Laskar, J., P. Robutel, F. Joutel, M. Gastineau, A. C. M. Correia, and B. Levrard (2004), A long term numerical solution for the insolation quantities of the Earth, *Astron. Astrophys.*, *428*(1), 261–285, doi:10.1051/0004-6361:20041335.

Laskar, J., A. Fienga, M. Gastineau, and H. Manche (2011), La2010: A new orbital solution for the long term motion of the Earth, *Astron. Astrophys.*, *532*, A89, doi:10.1051/0004-6361/201116836.

Lawver, L. A., and L. M. Gahagan (2003), Evolution of Cenozoic seaways in the circum-Antarctic region, *Palaeogeogr. Palaeoclimatol. Palaeoecol.*, *198*, 11–37, doi:10.1016/S0031-0182(03)00392-4.

Le Provost, C., M. L. Genco, F. Lyard, P. Vincent, and P. Canceil (1994), Spectroscopy of the world ocean tides from a finite element hydro dynamic model, *J. Geophys. Res.*, *99*(C12), 24,777–24,797.

Lee, H.-C., A. Rosati, and M. J. Spelman (2006), Barotropic tidal mixing effects in a coupled climate model: Oceanic conditions in the Northern Atlantic, *Ocean Modell.*, *11*, 464–477, doi:10.1016/j.ocemod.2005.03.003.

Li, C., J.-S. von Storch, and J. Marotzke (2012), Deep-ocean heat uptake and equilibrium climate response, *Clim. Dyn.*, *40*, 1071–1086, doi:10.1007/s00382-012-1350-z.

Livermore, R., A. Nankivell, G. Eagles, and P. Morris (2005), Paleogene opening of Drake Passage, *Earth Planet. Sci. Lett.*, *236*(1–2), 459–470, doi:10.1016/j.epsl.2005.03.027.

Loptson, C. A., D. J. Lunt, and J. E. Francis (2014), Investigating vegetation-climate feedbacks during the early Eocene, *Clim. Past*, *10*(2), 419–436, doi:10.5194/cp-10-419-2014.

Lucarini, V., and G. L. Russell (2002), Comparison of mean climate trends in the Northern Hemisphere between National Centers for Environmental Prediction and two atmosphere-ocean model forced runs, *J. Geophys. Res.*, *107*(D15), 4269, doi:10.1029/2001JD001247.

Lunt, D. J., P. J. Valdes, T. D. Jones, A. Ridgwell, A. M. Haywood, D. N. Schmidt, R. Marsh, and M. Maslin (2010), CO_2-driven ocean circulation changes as an amplifier of Paleocene-Eocene thermal maximum hydrate destabilization, *Geology*, *38*(10), 875–878, doi:10.1130/G31184.1.

Lunt, D. J., et al. (2012), A model data comparison for a multi-model ensemble of early Eocene atmosphere ocean simulations: EoMIP, *Clim. Past*, *8*(5), 1717–1736, doi:10.5194/cp-8-1717-2012.

Marinov, I., and A. Gnanadesikan (2011), Changes in ocean circulation and carbon storage are decoupled from air-sea CO_2 fluxes, *Biogeosciences*, *8*, 505–513, doi:10.5194/bg-8-505-2011.

Marinov, I., A. Gnanadesikan, J. L. Sarmiento, J. R. Toggweiler, M. Follows, and B. K. Mignone (2008), Impact of oceanic circulation on biological carbon storage in the ocean and atmospheric, *Global Biogeochem. Cycles*, *22*, GB3007, doi:10.1029/2007GB002958.

Marsland, S., H. Haak, J. H. Jungclaus, M. Latif, and F. Röske (2003), The Max-Planck-Institute global ocean/sea ice model with orthogonal curvilinear coordinates, *Ocean Modell.*, *5*(2), 91–127, doi:10.1016/S1463-5003(02)00015-X.

McCarthy, G., D. Smeed, W. Johns, E. Frajka-Williams, B. Moat, D. Rayner, M. Baringer, C. Meinen, J. Collins, and H. Bryden (2015), Measuring the Atlantic Meridional overturning circulation at 26°N, *Prog. Oceanogr.*, *130*, 91–111, doi:10.1016/j.pocean.2014.10.006.

Müller, M., H. Haak, J. H. Jungclaus, J. Sündermann, and M. Thomas (2010), The effect of ocean tides on a climate model simulation, *Ocean Modell.*, *35*(4), 304–313, doi:10.1016/j.ocemod.2010.09.001.

Munk, W., F. Snodgrass, and M. Wimbush (1970), Tides off-shore: Transition from California Coastal to Deep-Sea Waters, *Geophys. Fluid Dyn.*, *1*, 161–235, doi:10.1080/03091927009365772.

Nunes, F., and R. D. Norris (2006), Abrupt reversal in ocean overturning during the Palaeocene/Eocene warm period, *Nature*, *439*(7072), 60–63, doi:10.1038/nature04386.

Pacanowski, R. C., and S. G. Philander (1981), Parameterization of vertical mixing in numerical models of tropical oceans, *J. Phys. Oceanogr.*, *11*(11), 1443–1451.

Pagani, M., et al. (2006), Arctic hydrology during global warming at the Palaeocene/Eocene thermal maximum, *Nature*, *442*(7103), 671–675, doi:10.1038/nature05043.

Pak, D. K., and K. G. Miller (1992), Paleocene to Eocene benthic foraminiferal isotopes and assemblages: Implications for deepwater circulation, *Paleoceanography*, *7*(4), 405–422.

Parke, M. E. (1982), O_1, P_1, N_2 models of the global ocean tide on an elastic earth plus surface potential and spherical harmonic decompositions for M_2, S_2, and K_1, *Mar. Geod.*, *6*(1), 35–81.

Pearson, P. N., and M. R. Palmer (2000), Atmospheric carbon dioxide concentrations over the past 60 million years, *Nature*, *406*(6797), 695–699, doi:10.1038/35021000.

Poulsen, C. J., E. J. Barron, M. A. Arthur, and W. H. Peterson (2001), Response of the mid-Cretaceous global oceanic circulation to tectonic and CO_2 forcings, *Paleoceanography*, *16*(6), 576–592.

Purser, R. J., and L. M. Leslie (1988), A semi-implicit, semi-lagrangian finite-difference scheme using high-order spatial differencing on a nonstaggered grid, *Mon. Weather Rev.*, *116*(10), 2069–2080.

Raddatz, T., C. H. Reick, W. Knorr, J. Kattge, E. Roeckner, R. Schnur, K.-G. Schnitzler, P. Wetzel, and J. H. Jungclaus (2007), Will the tropical land biosphere dominate the climate-carbon cycle feedback during the twenty-first century?, *Clim. Dyn.*, *29*(6), 565–574, doi:10.1007/s00382-007-0247-8.

Robinson, I. S. (1981), Tidal vorticity and residual circulation, *Deep Sea Res.*, *28A*(3), 195–212.

Roeckner, E., et al. (2003), The atmospheric general circulation model ECHAM5: Part 1. Model description, *Tech. Rep. 349*, DKRZ, Max-Planck-Institut für Meteorologie, Hamburg, Germany.

Roeckner, E., R. Brokopf, M. Esch, M. Giorgetta, S. Hagemann, L. Kornblueh, E. Manzini, U. Schlese, and U. Schulzweida (2004), The atmospheric general circulation model ECHAM5: Part II, *Tech. Rep. 354*, DKRZ, Max-Planck-Institut für Meteorologie, Hamburg, Germany.

Rose, B. E., and D. Ferreira (2013), Ocean heat transport and water vapor greenhouse in a warm equable climate: A new look at the low gradient paradox, *J. Clim.*, *26*, 2117–2136, doi:10.1175/JCLI-D-11-00547.1.

Royer, D. L. (2006), CO_2-forced climate thresholds during the Phanerozoic, *Geochim. Cosmochim. Acta*, *70*(23), 5665–5675, doi:10.1016/j.gca.2005.11.031.

Royer, D. L., S. L. Wing, D. J. Beerling, D. W. Jolley, P. L. Koch, L. J. Hickey, and R. A. Berner (2001), Paleobotanical evidence for near present-day levels of atmospheric CO_2 during part of the tertiary, *Science*, *292*(5525), 2310–2313, doi:10.1126/science.292.5525.2310.

Scher, H. D., and E. E. Martin (2006), Timing and climatic consequences of the opening of Drake Passage, *Science*, *312*(5772), 428–30, doi:10.1126/science.1120044.

Sewall, J. O., L. C. Sloan, M. Huber, and S. L. Wing (2000), Climate sensitivity to changes in land surface characteristics, *Global Planet. Change*, *26*(4), 445–465, doi:10.1016/S0921-8181(00)00056-4.

Sexton, P. F., R. D. Norris, P. A. Wilson, H. Pälike, T. Westerhold, U. Röhl, C. T. Bolton, and S. Gibbs (2011), Eocene global warming events driven by ventilation of oceanic dissolved organic carbon, *Nature*, *471*(7338), 349–352, doi:10.1038/nature09826.

Shellito, C. J., J.-F. Lamarque, and L. C. Sloan (2009), Early Eocene Arctic climate sensitivity to pCO_2 and basin geography, *Geophys. Res. Lett.*, *36*, L09707, doi:10.1029/2009GL037248.

Sloan, L. C., and D. Pollard (1998), Polar stratospheric clouds: A high latitude warming mechanism in an ancient greenhouse world, *Geophys. Res. Lett.*, *25*(18), 3517–3520, doi:10.1029/98GL02492.

Sloan, L. C., J. C. Walker, and T. C. Moore (1995), Possible role of oceanic heat transport in early Eocene climate, *Paleoceanography*, *10*(2), 347–56.

Sluijs, A., et al. (2006), Subtropical Arctic Ocean temperatures during the Palaeocene/Eocene thermal maximum, *Nature*, *441*(7093), 610–613, doi:10.1038/nature04668.

Steele, M., R. Morley, and W. Ermold (2001), PHC: A global ocean hydrography with a high-quality Arctic Ocean, *J. Clim.*, *14*, 2079–2087.

Stepanek, C., and G. Lohmann (2012), Modelling mid-Pliocene climate with COSMOS, *Geosci. Model Dev.*, *5*(5), 1221–1243, doi:10.5194/gmd-5-1221-2012.

Stickley, C. E., K. St John, N. Koç, R. W. Jordan, S. Passchier, R. B. Pearce, and L. E. Kearns (2009), Evidence for middle Eocene Arctic sea ice from diatoms and ice-rafted debris, *Nature*, *460*(7253), 376–379, doi:10.1038/nature08163.

Thomas, D. J., R. Korty, M. Huber, J. A. Schubert, and B. Haines (2014), Nd isotopic structure of the Pacific Ocean 70–30 Ma and numerical evidence for vigorous ocean circulation and ocean heat transport in a greenhouse world, *Paleoceanography*, *29*, 454–469, doi:10.1002/2013PA002535.

Thomas, M., J. Sündermann, and E. Maier-Reimer (2001), Consideration of ocean tides in an OGCM and impacts on subseasonal to decadal polar motion excitation, *Geophys. Res. Lett.*, *28*(12), 2457–2460.

Tripati, A. K., and H. Elderfield (2005), Deep-sea temperature and circulation changes at the Paleocene-Eocene Thermal Maximum, *Science*, *308*(5730), 1894–1898, doi:10.1126/science.1109202.

Uenzelmann-Neben, G., T. Weber, J. Gruetzner, and M. Thomas (2016), Transition from the Cretaceous ocean to Cenozoic circulation in the western South Atlantic: A twofold reconstruction, *Tectonophysics*, doi:10.1016/j.tecto.2016.05.036.

Weber, T. (2016), Impact of ocean tides on the climate system during the pre-industrial period, the early Eocene, and the Albian, PhD thesis, Dep. of Earth Sci., Freie Universität, Berlin. [Available at http: //www.diss.fu-berlin.de/diss/receive/FUDISS_thesis_000000100930.]

Weber, T., and M. Thomas (2017), Tidal influence on the ocean during the early Eocene, GFZ Data Serv., doi:10.5880/GFZ.1.3.2017.001.

Winguth, A., C. J. Shellito, C. Shields, and C. Winguth (2010), Climate response at the Paleocene-Eocene thermal maximum to greenhouse gas forcing—A model study with CCSM3, *J. Clim.*, *23*(10), 2562–2584, doi:10.1175/2009JCLI3113.1.

Winguth, A. M. E., E. Thomas, and C. Winguth (2012), Global decline in ocean ventilation, oxygenation, and productivity during the Paleocene-Eocene Thermal Maximum: Implications for the benthic extinction, *Geology*, *40*(3), 263–266, doi:10.1130/G32529.1.

Yanagi, T. (1976), Fundamental study on the tidal residual circulation—I, *J. Oceanogr. Soc. Jpn.*, *32*(5), 199–208, doi:10.1007/BF02107122.
Zachos, J. C., L. D. Stott, and K. C. Lohmann (1994), Evolution of early Cenozoic marine temperatures, *Paleoceanography*, *9*(2), 353–387.
Zeebe, R. E., J. C. Zachos, and G. R. Dickens (2009), Carbon dioxide forcing alone insufficient to explain Palaeocene-Eocene Thermal Maximum warming, *Nat. Geosci.*, *2*(8), 576–580, doi:10.1038/ngeo578.
Zhang, Z. S., K. Nisancioglu, M. Bentsen, J. Tjiputra, I. Bethke, Q. Yan, B. Risebrobakken, C. Andersson, and E. Jansen (2012), Pre-industrial and mid-Pliocene simulations with NorESM-L, *Geosci. Model Dev.*, *5*(2), 523–533, doi:10.5194/gmd-5-523-2012.
Zimmerman, J. T. F. (1981), Dynamics, diffusion and geomorphological significance of tidal residual eddies, *Nature*, *290*, 549–555.